

Journal of Materials Chemistry A

Accepted Manuscript



This is an *Accepted Manuscript*, which has been through the Royal Society of Chemistry peer review process and has been accepted for publication.

Accepted Manuscripts are published online shortly after acceptance, before technical editing, formatting and proof reading. Using this free service, authors can make their results available to the community, in citable form, before we publish the edited article. We will replace this *Accepted Manuscript* with the edited and formatted *Advance Article* as soon as it is available.

You can find more information about *Accepted Manuscripts* in the [Information for Authors](#).

Please note that technical editing may introduce minor changes to the text and/or graphics, which may alter content. The journal's standard [Terms & Conditions](#) and the [Ethical guidelines](#) still apply. In no event shall the Royal Society of Chemistry be held responsible for any errors or omissions in this *Accepted Manuscript* or any consequences arising from the use of any information it contains.

ARTICLE

Hydrothermal Synthesis, Structure Refinement, and Electrochemical Characterization of $\text{Li}_2\text{CoGeO}_4$ as an Oxygen Evolution Catalyst

Cite this: DOI: 10.1039/x0xx00000x

Received 00th January 2012,
Accepted 00th January 2012

DOI: 10.1039/x0xx00000x

www.rsc.org/

Kenneth J. McDonald,^a Ruigang Zhang,^a Chen Ling,^a Li Qin Zhou,^a Ruibo Zhang,^b M. Stanley Whittingham^b, and Hongfei Jia^{a*}

Lithium cobalt germanate ($\text{Li}_2\text{CoGeO}_4$) has been synthesized for the first time by a hydrothermal method at 150 °C. Elemental composition, morphology, and crystal structure of this compound were characterized by various analytical techniques including SEM, TEM, ICP, and XRD analyses. Structure refinement and DFT calculation suggests the crystal structure of the resulting $\text{Li}_2\text{CoGeO}_4$ from hydrothermal synthesis is isostructural to $\text{Li}_2\text{ZnGeO}_4$, significantly different from previous reports. Electrochemical studies confirmed $\text{Li}_2\text{CoGeO}_4$ as an active catalyst for oxygen evolution reaction (OER). In alkaline electrolyte (0.1 M NaOH), rotating disk electrodes made with $\text{Li}_2\text{CoGeO}_4$ as catalyst have a Tafel slope of c.a. 67 mV/dec and an overpotential of 330 mV at 50 $\mu\text{A}/\text{cm}^2_{\text{cat}}$, about 90 mV less than the electrodes containing another known OER catalyst, Co_3O_4 . Further characterization with cyclic voltammetry, high resolution transmission electron microscopy, X-ray photoelectron spectroscopy and elemental analyses revealed the oxidation of Co from 2+ to 3+ during the reaction along with significant surface amorphization and loss of Li and Ge from the catalyst.

Introduction

Water splitting and artificial photosynthesis systems are currently under intensified study for the conversion and storage of solar energy into chemical fuels.¹⁻⁷ However, the efficiency of those processes is often limited by the sluggish kinetics of the four proton-coupled electron transfers required for the oxygen evolution reaction (OER).⁸ IrO_2 and RuO_2 are known catalysts that can effectively reduce activation barriers for OER, but their material cost is too high. Therefore, it is still essential to find low-cost catalyst alternatives that are feasible for large scale applications, such as those targeting to reduce atmospheric CO_2 level and remediate the risk of global climate change.³

Among the many recent efforts focusing on oxide-based materials, there has been a growing interest to examine lithium containing oxides, previously known as cathode materials of lithium ion batteries, for use as OER catalysts. Recently, LiCoO_2 and LiCoPO_4 were studied thoroughly for OER catalysis in both alkaline and neutral electrolytes.⁹ A combination of structural and electrochemical analyses revealed the important role of catalyst surface properties to their activities. Likewise, $\text{LiMn}_{1.5}\text{Ni}_{0.5}\text{O}_4$ was used to systematically investigate the effect of surface planes/facets on OER activity and it has been found that catalyst activity increased in the order of truncated octahedral < cubic < spherical < octahedral surface structures.¹⁰ More recently, a new catalyst based on lithium manganese pyrophosphate was studied for water

oxidation at neutral pH, from which the role of Mn valency in OER catalysis was elucidated via controlled delithiation ($\text{Li}_{2-x}\text{MnP}_2\text{O}_7$, $x=0, 0.3, 0.5, 1$).¹¹

$\text{Li}_2\text{CoGeO}_4$ (LCG) belongs to the same family of compounds as $\text{Li}_2\text{CoSiO}_4$ (LCS) with structure derived from Li_3PO_4 . Recently the synthesis, crystal structure, and electrochemical properties of LCS were extensively investigated for lithium ion battery application.¹²⁻¹⁵ However, for LCG, there has been no dedicated study, except for a few very old reports.¹⁶⁻¹⁹ Herein, we report for the first time hydrothermal synthesis of $\text{Li}_2\text{CoGeO}_4$, as well as the characterization of its material properties and use as OER catalyst. Structural refinement and DFT calculation were also conducted to clarify the ambiguity on its crystal structure from previous studies.

Experimental

Materials synthesis. LCG was prepared by hydrothermal synthesis from GeO_2 (Sigma-Aldrich), $\text{LiOH}\cdot\text{H}_2\text{O}$ (Sigma-Aldrich), and $\text{CoCl}_2\cdot 6\text{H}_2\text{O}$ (Sigma-Aldrich). Into an 80 mL Teflon lined autoclave 0.0125 mol of GeO_2 and 0.05 mol of $\text{LiOH}\cdot\text{H}_2\text{O}$ were added to 20 mL of deionized water. In a separate beaker 0.0125 mol of $\text{CoCl}_2\cdot 6\text{H}_2\text{O}$ was dissolved in a mixture of ethylene glycol (10 ml) and H_2O (10 ml), and then added to the Teflon autoclave. The autoclave was then sealed and heated to 150 °C for 12 h. The resulting product was

ARTICLE

filtered, washed with deionized water, and dried under vacuum (60 °C, 12 h). After drying, the powder was ground using a mortar and pestle then used for characterization.

Characterization of materials properties. Morphology of hydrothermal synthesized LCG (hydro-LCG) was studied on a JEOL 7800 field emission scanning electronic microscope (SEM) and JEOL 3011 high resolution transmission electronic microscope (HR-TEM). Elemental composition was determined by inductively coupled plasma (ICP, Evan Analytical) analyses. The structure of the samples was characterized by powder X-ray diffraction (XRD), using a Rigaku Smart Lab θ - θ powder diffractometer equipped with a Cu K α radiation ($\lambda = 1.54178 \text{ \AA}$) source. The data was collected with a step size of 0.02° and exposure time of 12 s. Rietveld refinement of the powder XRD patterns was performed using the GSAS/EXPGUI package.²⁰ X-ray photoelectron spectroscopy (XPS) analysis was conducted on a PHI 5000 VersaProbe II system to verify the valance state of Co for hydro-LCG and Co₃O₄. High resolution Co 2p scans were performed with 23.5 eV pass energy and a scan step of 0.1 eV. Specific surface area of hydro-LCG was measure by nitrogen adsorption and desorption (BET) using a Micromeritics ASAP 2020 Surface Area and Porosity Analyser.

Electrode Preparation and Electrochemical Measurements. Electrochemical experiments were performed in 0.1 M NaOH solution at room temperature in three electrode cells using a VSP multichannel potentiostat (Bio-logic). Working electrodes for cyclic voltammetry (CV), galvanostatic and Tafel analyses were prepared using a previously reported procedure.^{21,22} A catalyst ink was first prepared by sonicating a mixture of catalyst, acid-treated carbon black (CB, Alfa Aesar), Na⁺-exchanged Nafion® solution (5 wt%, Ion Power) with tetrahydrofuran (THF, Sigma-Aldrich), and then drop-cast (10 μL) onto pre-polished glassy carbon disk electrodes (5 mm in diameter, Pine Instruments). The catalyst film was allowed to dry at room temperature overnight and the final composition of the film was expected to be 100, 20, and 20 $\mu\text{g}/\text{cm}^2$ for hydro-LCG, CB, and Nafion®, respectively. Working electrodes rotated at 1600 rpm using a rotating disc electrode system (Pine Instruments). The counter electrode was a Pt coil isolated from the main electrochemical cell using a fritted glass tube. All potentials were measured versus a Ag/AgCl (4 M KCl) reference electrode, corrected for IR drop, and converted to reversible hydrogen electrode (RHE) for easy discussion and comparison to previous literature. Electrodes for XPS, HR-TEM and SEM EDX analyses were prepared by depositing hydro-LCG particles directly on Indium Tin Oxide (ITO) coated glass slides (10x45 mm, LGA) via dip coating from a catalyst suspension in ethanol (1.0 mg/ml). To confirm O₂ product and estimate Faraday efficiency, bulk electrolysis was performed with a hydro-LCG/ITO electrode in a two-chamber air-tight electrochemical cell. An optical O₂ sensor (Ocean optics, Foxy-R) was used to monitor O₂ concentration in the headspace of the anode chamber, from which the total amount of O₂ product was estimated via Henry's law.

DFT calculations. DFT calculations were performed with the Vienna *ab initio* Simulation Package (VASP) used projector augmented waves (PAW) pseudopotentials and the exchange-correlation functionals parameterized by Perdew, Burke, and Ernzerhof for the generalized gradient approximation (GGA).²³⁻²⁶ A cutoff energy of 500.0 eV was used to ensure numerical

Journal Name

convergence to less than 5 meV per LCG formula. The Gamma centered k-point mesh was sampled with the density of at least 0.03 \AA^{-1} . GGA+U method was used to treat the static correlations by introducing a Hubbard type potential to describe the d-part of the Hamiltonian. The value of effective U (U-J) is set to be 5.7 eV as suggested in previous reports for Co.²⁷ After the crystal structure is relaxed, powder X-ray diffraction pattern is simulated with Mercury code.

Results and discussion

Previous report of synthesizing LCG used high temperature solid state process, involving an initial heating of the mixture of Li₂CO₃, CoO, and GeO₂ at 700 °C for ~2-3 h and then subsequent overnight sintering at 1000 °C to complete the reaction.¹⁶ In an attempt to use more mild synthesis conditions, LCG in this work was prepared via a hydrothermal method for the first time, by heating reaction precursors (stoichiometric amount of CoCl₂ and GeO₂ with excess LiOH) in an ethylene glycol/water solution at 150 °C for 12 h. Figure 1 shows SEM and TEM images of the resulting hydro-LCG product. SEM images of the hydro-LCG powder (Figure 1(a,b)) consists of particles with a flower-like morphology with size in the range of a few hundred nanometers. It can be seen from the TEM image (Figure 1(c)) that each individual particle is composed of smaller triangular shaped petals. High resolution-TEM images along with the electron diffraction pattern confirmed that these triangular petals are highly crystalline (Figure 1(d)).

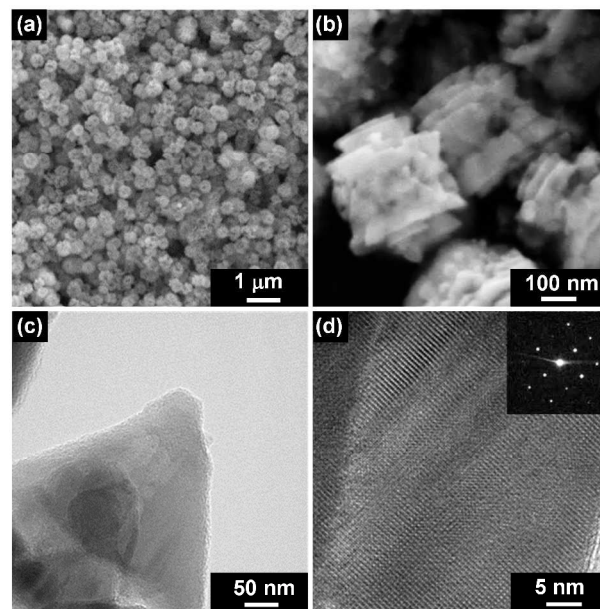


Figure 1. Morphology of hydrothermally synthesized hydro-LCG: (a, b) SEM images of the powder sample, (c) TEM image of a selected triangular petal and (d) high resolution TEM image showing the crystal lattice and electron diffraction patterns (insert).

Li₂MXO₄ has a large family of structures comprised of distorted hexagonal close packing oxygen ions with half of the tetrahedral sites occupied by cations (Li, M, and X). To the best of our knowledge, the crystal structure of LCG has only been discussed in three publications. Glasser et al. reported the polymorph γ_{II} structure with space group Pnma (PDF 04-002-

Journal Name

4634),¹⁸ and Tarte et al. assigned their structure to the β_{II} polymorph, space group Pmn2₁ (PDF 04-001-8430),¹⁹ whereas West et al. proposed that the structure of LCG could be orthorhombic but did not assign any space group.¹⁷ However, the XRD pattern obtained from hydro-LCG in this study, as shown in Figure 2, cannot be indexed to any of the previously reported crystal structures. ICP analysis confirmed the Li:Co:Ge ratio of hydro-LCG was 2:1:1 eliminating the possibility of a non-stoichiometric cation composition that may create structural differences. Therefore, we postulate hydro-LCG may have a different crystal structure from those reported previously.

ARTICLE

β_I , β_{II} , and γ_{II} models led to unacceptable results with the R_p and R_{wp} typically larger than 15% and 25%, respectively (ESI S1). The γ_{II} polymorph was unable to generate any results likely due to a large difference in structure.

Although the LCS and LCG structures are isoelectronic with one another, the size discrepancy between Si^{4+} (0.26 Å) and Ge^{4+} (0.39 Å) could lead to large differences in refinement between the different polymorphs of LCS and hydro-LCG.²⁸ To determine if this was the case, additional refinements were conducted by isoelectronically substituting two ions closer in size Co^{2+} (0.58 Å) for Zn^{2+} (0.60 Å) in a Li_2ZnGeO_4 (LZG) model system (Space group $P_n(7)$) (PDF#04-015-4929).²⁹ The Rietveld refinement of the hydro-LCG diffraction pattern, using starting coordinates from LZG structure, gave acceptable fitting results, as shown in Figure 2. Table 1 summarizes refined crystallographic parameters for hydro-LCG.

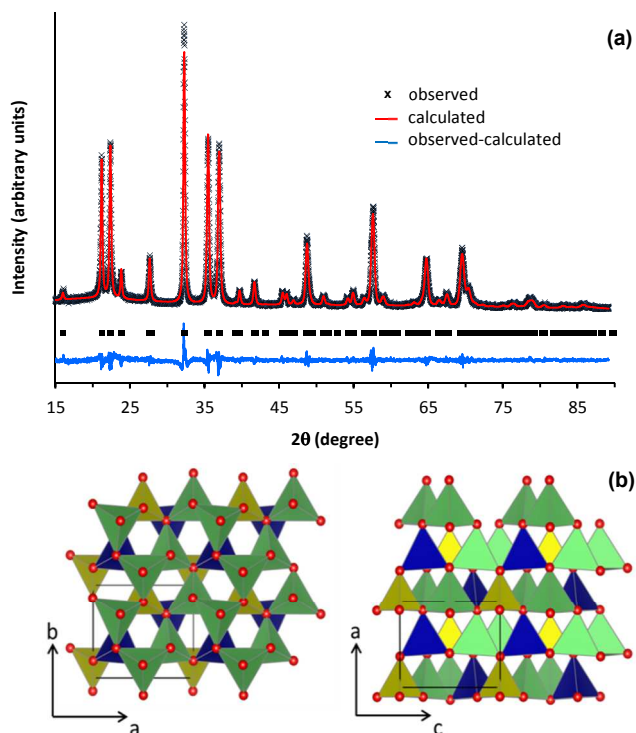


Figure 2. (a) Refined powder x-ray diffraction pattern for hydro-LCG, space group $P_n(7)$. (b) Schematic visualization of hydro-LCG crystal structure in the (left) [001] and (right) [010] directions. Li, Co, and Ge tetrahedral with connecting oxygen atoms (red circles) are represented by green, blue, and yellow colour, respectively.

In order to shed light on the structure analysis, Rietveld refinements were performed using the reported LCG models (β_{II} and γ_{II}). Additionally, two other well-known structure models based on LCS (β_I , space group Pbn2₁ and γ_0 space group $P2_1/n$), an isoelectronic compound to LCG, were examined by substituting Ge^{4+} for Si^{4+} .¹⁵ After refinement the

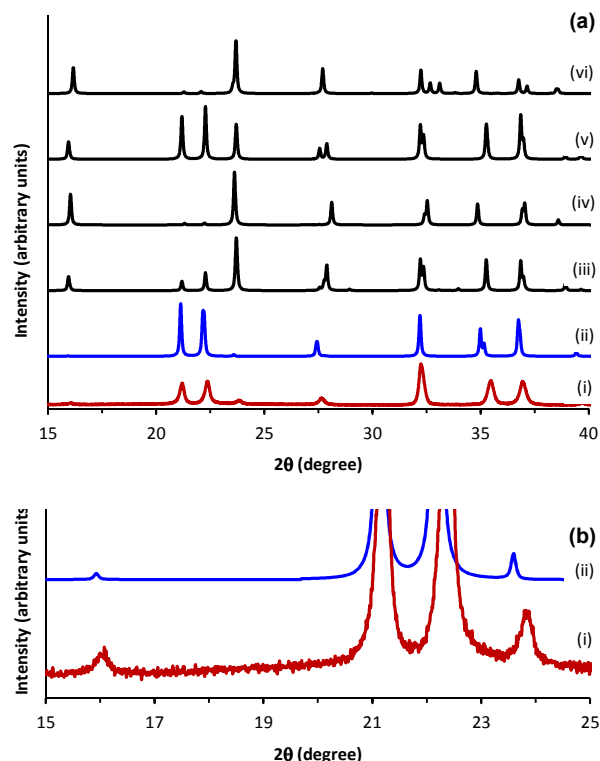


Figure 3. (a) XRD patterns of LCG in the range of 15-45° two theta: (i) measured experimentally, as well as simulated using (ii) LZG, (iii) β_I , (iv) β_{II} , (v) γ_0 , and (vi) γ_{II} . (b) Enhanced view between 15-25° two theta of (i) experimentally prepared and (ii) LZG simulated LCG showing the presence of weak peaks near 16° and 24° for both patterns. Full range patterns can be found in ESI S2.

Table 1. Refined crystallographic parameters for LCG space group P_n *

atom	<i>a</i>	<i>b</i>	<i>c</i>	Occupancy	U_{iso}
Li1	0.4461	0.1495	-0.06567	1	0.01531
Li2	0.9317	0.2828	0.3756	1	0.04831
Co	0.2277	0.3281	0.4813	1	0.01889
Ge	-0.01900	0.1872	-0.03759	1	0.05976
O1	0.8300	0.36075	0.4072	1	0.0956
O2	0.2049	0.6774	0.3800	1	0.00210
O3	1.0014	-0.1522	0.5077	1	0.02680
O4	0.1681	0.2875	0.9073	1	0.00917

* $R_p = 7.58\%$, $R_{wp} = 9.94\%$, $a = 6.3505(9)$ Å, $b = 5.4745(3)$ Å, $c = 5.0062(5)$ Å, $V = 174.049(9)$ Å³, $\beta = 90.218$, $\rho_{calc} = 4.039$ g/cm³

ARTICLE

In order to further verify the crystal structure for hydro-LCG, DFT relaxations were performed with five structure models, including the earlier mentioned β_1 , β_{11} , γ_0 , γ_{11} , and LZG. The fully relaxed structures were used to simulate the powder X-ray diffraction pattern. Figure 3 shows the X-ray diffraction pattern of hydro-LCG collected experimentally compared to the simulated ones. Several characteristic differences were observed. First, the structure relaxed with LZG model showed minimum peak intensity around 16° , while all the others showed diffraction peaks with considerable intensity at the same range. The experimental pattern showed a weak peak at 15.9° , which was only consistent with the LZG model (Figure 3b). Second, the experimental pattern showed three diffraction peaks between 20 - 25° , with two peaks at 21.2° and 22.3° at similar intensity and the third peak with much lower intensity at 23.7° . This characteristic was obviously only captured by the LZG model, while in all the other models the intensities of these peaks were in different ratios. Third, at 32° there was only one single peak on the experimental pattern, which again agrees the best only with the LZG model. The peak splitting at this range was noticed in all other models. These characteristics strongly support the conclusion that hydro-LCG is actually isostructural to LZG. Interestingly, the calculated energy was also the lowest for LZG model, although the energy difference was not huge (30-240 meV per formula, see ESI S3 for details).

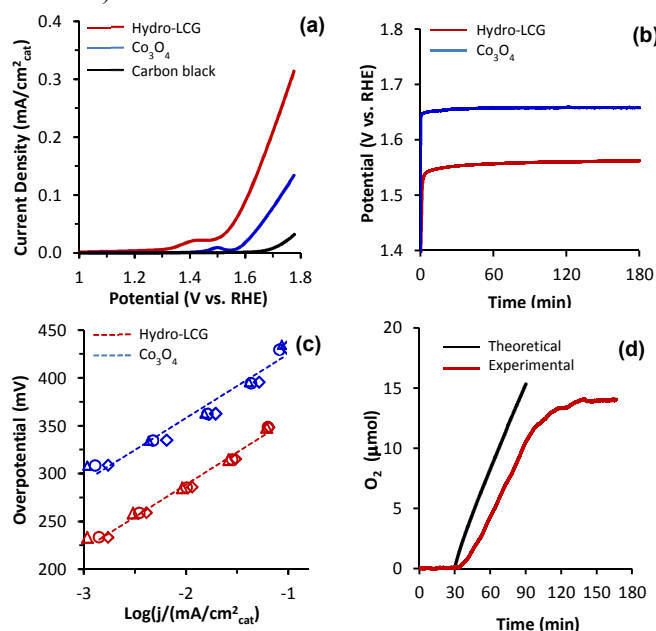


Figure 4. Comparison of hydro-LCG and Co₃O₄ as OER catalysts in 0.1 M NaOH. (a) LSVs measured at 1 mV s⁻¹; (b) galvanostatic measurements at 50 μA/cm^{2_cat}; (c) steady-state Tafel plots based on the average of three independent measurements (labeled with Δ, ○ and ◇, respectively). Catalyst loading: 0.1 mg/cm^{2_geo}; Current density was normalized based on specific surface area of the catalysts, 23.0 and 45.1 m²/g, for hydro-LCG, Co₃O₄, and carbon black (control, 77.0 m²/g), respectively. Solution ionic resistances were compensated at ~55 and ~60 Ω for hydro-LCG and Co₃O₄ RDEs, respectively. (d) O₂ evolution from a dip coated hydro-LCG/ITO electrode at 1.63 V (vs. RHE), applied from 30 to 90 min. The O₂ product was measure by an optical O₂ sensor. Theoretical value was calculated based on the accumulated charges transferred through the working electrode.

Hydro-LCG is a potential catalyst for OER similar to other lithium cobalt compounds.⁹ To assess its activity, hydro-LCG

Journal Name

was deposited on glassy carbon rotating disk electrodes (RDEs) by drop-casting as catalyst/carbon black/Nafion composite thin films. Electrodes containing commercially purchased Co₃O₄ nanoparticles, another known OER catalyst, were also prepared and tested using the same procedure for comparison purposes.^{30,31}

All electrochemical characterizations were conducted in alkaline electrolyte (0.1 M NaOH) saturated with oxygen. Linear sweep voltammograms (LSVs) at a scan rate of 1 mV s⁻¹ on electrodes with and without catalysts are shown in Figure 4 (a). Catalytic activity of hydro-LCG and Co₃O₄ is evident as a significant increase in current at potentials more positive than 1.55 V was observed for both catalysts compared to a control electrode without catalyst. It can be seen that hydro-LCG has an earlier onset for water oxidation and is able to achieve higher currents as the applied positive potential increases. Such a higher activity of hydro-LCG is further confirmed with galvanostatic analysis. At a constant current of 50 μA/cm^{2_cat}, an overpotential of 330 mV (1.56 V vs. RHE) for OER was observed from hydro-LCG electrodes, as compared to 420 mV (1.65 V vs. RHE) from Co₃O₄ (Figure 4(b)). Figure 4(c) shows Tafel plots of the two catalysts obtained under steady state conditions. Tafel slopes, determined from the average of three independent tests, are calculated as 67 and 66 mV/dec, for hydro-LCG and Co₃O₄, respectively, similar to those reported on LiCoO₂ and LiCoPO₄.⁹ Remarkably, the exchange current density from hydro-LCG electrode was estimated as 5.6x10⁻¹⁰ A/cm^{2_cat}, about one order of magnitude higher than that of Co₃O₄ (4.3x10⁻¹¹ A/cm^{2_cat}). To verify O₂ production, bulk electrolysis was conducted in an air-tight, 2-chamber electrochemical cell equipped with an optical O₂ sensor. As shown in Figure 4(d), once the applied potential was switched on (at 30 min), the generation of O₂ product was evident, and the Faraday's efficiency is estimated as ~90%.

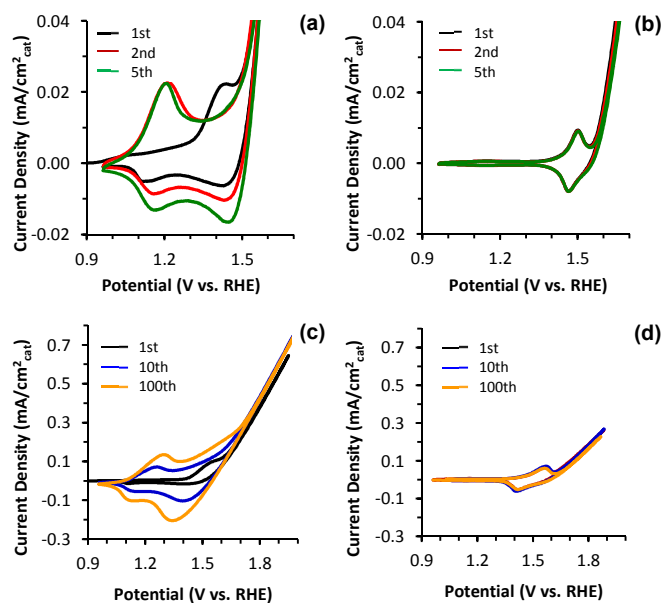


Figure 5. Cyclic voltammograms at a 1 mV s⁻¹ scan rate for (a) hydro-LCG and (b) Co₃O₄ as well as a 10 mV s⁻¹ scan rate for (c) hydro-LCG and (d) Co₃O₄ in 0.1 M NaOH. Data are plotted at different scale to better visualize the redox waves. Please refer to ESI S4 for comparison at same scale.

LSV of hydro-LCG shows a characteristic oxidation peak around 1.41 V vs. RHE prior to OER current, which was also

Journal Name

seen as a redox couple from cyclic voltammetry (CV) analysis (Figure 5(a)). Such a transition very likely corresponds to $\text{Co}^{2+}/\text{Co}^{3+}$ oxidation, as reported from many Co-containing OER catalysts.^{32, 33} The $E_{1/2}$ of this redox couple is 1.43 V at first CV cycle and downshifted to ~ 1.20 V at the 2nd cycle and thereafter. Similar pre-OER redox peaks were also observed from Co_3O_4 (Figure 5(b)), but they were at higher potentials and appeared to be stable during the CV cycles. It is unclear if the lower redox potential as observed from hydro-LCG contributes to its high activity, which remains a subject for future study.

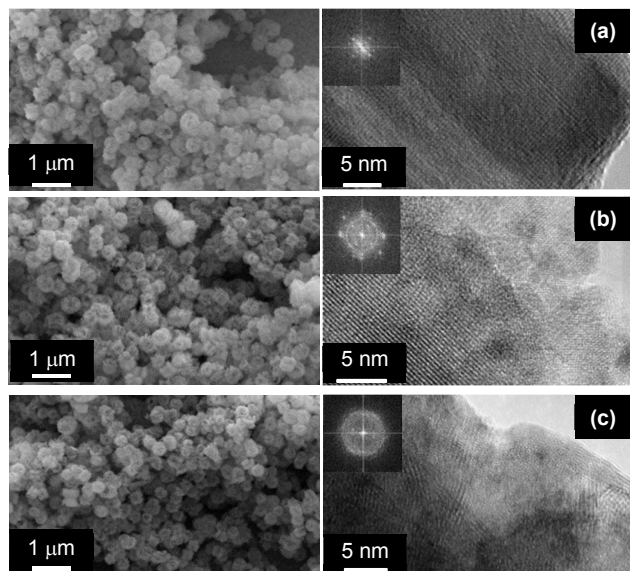


Figure 6. SEM (left column) and HR-TEM (right column) images of dip coated pristine (a) and hydro-LCG on ITO electrodes after one (b) and one hundred (c) CV cycles. Inserts: fast Fourier transform (FFT) of catalyst surface regions. Scan rate: $10 \text{ mV}\cdot\text{s}^{-1}$.

Under galvanostatic condition (Figure 4(b)), the potential of both hydro-LCG and Co_3O_4 electrodes increased at the beginning and then became steady towards the end of the test. Stability of the catalysts was further investigated by 100 cycles of CV scan at a faster rate ($10 \text{ mV}\cdot\text{s}^{-1}$). An increase of pseudocapacitive currents was observed from hydro-LCG, while the catalytic current remained about the same (Figure 5(c)). The increase of pseudocapacitance was previously reported on LiCoPO_4 as OER catalyst, which was attributed to structural and chemical transformation of catalyst based on a thorough investigation using HR-TEM.⁹ Survey of hydro-LCG before and after CV cycles with SEM did not reveal much morphology change at μm -scale (Figure 6), although compositional change was very significant as observed by EDX analysis. Pristine hydro-LCG has a Ge:Co atomic ratio of 1:1, which did not change after being soaked in 0.1 M NaOH for 4 hr (about same time as it takes to complete 100 CV cycles at $10 \text{ mV}\cdot\text{s}^{-1}$). However, this ratio decreased to 0.14 ± 0.02 (average of eight independent spectra analyses) after 100 CV cycles, indicating an essential loss of Ge from the catalyst since cobalt is known not soluble at pH 13.⁴⁰ Furthermore, a loss of $\sim 50\%$ of Li was also detected from hydro-LCG by ICP analysis after 100 of cycles. Along with the compositional changes, HR-TEM images revealed profound differences from catalyst surface before and after CV cycles (Figure 6). While pristine hydro-LCG is highly crystalline, amorphization can be seen

ARTICLE

clearly from catalyst surface after even the first cycle of CV scan, and became much more severe after 100 cycles.

XPS analysis was conducted on fresh and used hydro-LCG electrodes to further probe the possible changes to the catalyst surface during OER. After being used for OER, the colour of the catalyst film changed from blue to dark brown (Figure 7). Co 2p spectrum from fresh hydro-LCG has a very characteristic Co^{2+} signal with two main peaks at 797.1 and 781.1 eV for the $2p_{1/2}$ and $2p_{3/2}$ regions and the corresponding satellite peaks at 802.7 and 786.8 eV, respectively. After use the hydro-LCG XPS spectra resembled closely to Co_3O_4 standard in the $2p_{3/2}$ and $2p_{1/2}$ regions with the positions of the main peaks shifting to lower energy and a decrease of relative intensity of satellite peaks to the main peaks (Figure 7). These changes typically indicate a transition from high spin Co^{2+} to Co^{3+} ,³⁴⁻³⁸ which also corresponds well with the previously reported colour change of other Co^{2+} containing OER that oxidize to Co^{3+} .^{22,39}

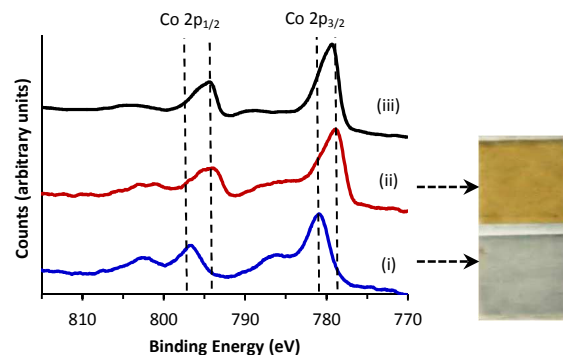


Figure 7. XPS spectra of dip coated hydro-LCG (i) before and (ii) after applying 1.7 V for 2 h as well as (iii) Co_3O_4 as a standard. Photos on right hand side show colour of the electrode before (top) and after (down) being used for OER.

Although collective evidences from CV, HR-TEM, XPS and compositional analyses suggest that structure and composition of hydro-LCG evolved during OER process, completely understanding the active site structure and reaction mechanism is not trivial and largely beyond the scope of this study. The initial oxidation of Co from $2+$ to $3+$, as observed from LSV and forward scan of 1st CV cycle, might have triggered the disruption of catalyst surface structure and the loss of Li and Ge. As such amorphization progresses deeper into bulk catalyst, it apparently did not create more active sites at outer layer of the catalyst because there was no increase of catalytic current, but resulted in larger area of internal grain boundaries, which corresponds to the rise of pseudocapacitance. In reference to a previous report of amorphization of LiCoO_2 and LiCoPO_4 for OER in alkaline electrolytes⁹, we believe the active sites of the evolved hydro-LCG resemble more to those from LiCoPO_4 , because of i) similar Tafel slopes, ii) significant loss of Ge or P during CV scans, iii) retention of about half of Li from hydro-LCG after 100 CV cycles, and most importantly, iv) the absence of a second pair of redox peaks at ~ 1.41 V vs. RHE observed as a distinct feature of amorphized LiCoO_2 .

Conclusions

We have shown that $\text{Li}_2\text{CoGeO}_4$ can be synthesized hydrothermally at a temperature much lower than previously

ARTICLE

reported solid state methods. The hydrothermally synthesized $\text{Li}_2\text{CoGeO}_4$ was found to be isostructural with $\text{Li}_2\text{ZnGeO}_4$, which is different from the previously reported two structure models. Electrochemical characterization confirmed $\text{Li}_2\text{CoGeO}_4$ was catalytically active towards OER in alkaline electrolyte with performance better than Co_3O_4 . Further characterization of the catalyst with CV, HR-TEM, XPS and elemental analyses revealed the oxidation of cobalt from 2+ to 3+ during OER process, along with significant surface amorphization and loss of Li and Ge from the catalyst.

Acknowledgements

The work at Binghamton was supported by the Assistant Secretary for Energy Efficiency and Renewable Energy, Office of Vehicle Technologies of the U.S. Department of Energy under contract no. DE-AC02-05CH11231, under the Batteries for Advanced Transportation Technologies (BATT) Program subcontract no. 6807148.

Notes and references

^a Materials Research Department, Toyota Research Institute of North America, 1555 Woodridge Ave., Ann Arbor, MI 48105, USA. E-mail: hongfei.jia@tema.toyota.com; Fax: +1-734-995-2549; Tel: +1-734-995-0183

^b Department of Chemistry and Materials Science, State University of New York, Binghamton, New York 13902-6000, USA

Electronic Supplementary Information (ESI) available: details of structure refinements using different space group models, full range XRD spectra from DFT calculations, energy calculated by DFT and galvanostatic analysis of hydro-LCG and Co_3O_4 at 50 $\mu\text{A}/\text{cm}^2_{\text{catalyst}}$. See DOI: 10.1039/b000000x/

- J. R. McKone, N. S. Lewis and H. B. Gray, *Chemistry of Materials*, 2013.
- M. G. Walter, E. L. Warren, J. R. McKone, S. W. Boettcher, Q. Mi, E. A. Santori and N. S. Lewis, *Chemical Reviews*, 2010, **110**, 6446-6473.
- N. S. Lewis and D. G. Nocera, *Proc. Natl. Acad. Sci. U.S.A.*, 2006, **103**, 15729-15735.
- B. A. Pinaud, J. D. Benck, L. C. Seitz, A. J. Forman, Z. Chen, T. G. Deutsch, B. D. James, K. N. Baum, G. N. Baum, S. Ardo, H. Wang, E. Miller and T. F. Jaramillo, *Energy & Environmental Science*, 2013, **6**, 1983-2002.
- T. Faunce, S. Styring, M. R. Wasielewski, G. W. Brudvig, A. W. Rutherford, J. Messinger, A. F. Lee, C. L. Hill, H. deGroot, M. Fontecave, D. R. MacFarlane, B. Hankamer, D. G. Nocera, D. M. Tiede, H. Dau, W. Hillier, L. Wang and R. Amal, *Energy & Environmental Science*, 2013, **6**, 1074-1076.
- W. Lubitz, E. J. Reijerse and J. Messinger, *Energy & Environmental Science*, 2008, **1**, 15-31.
- R. E. Blankenship, D. M. Tiede, J. Barber, et al. *Science*, 2011, **332**, 805-809.
- D. G. Nocera, *Acc. Chem. Res.*, 2012, **45**, 767-776.

Journal Name

- S. W. Lee, C. Carlton, M. Risch, Y. Surendranath, S. Chen, S. Furutsuki, A. Yamada, D. G. Nocera and Y. Shao-Horn, *Journal of the American Chemical Society*, 2012, **134**, 16959-16962.
- T. Maiyalagan, K. R. Chemelewski and A. Manthiram, *ACS Catalysis*, 2013, **4**, 421-425.
- J. Park, H. Kim, K. Jin, B. J. Lee, Y.-S. Park, H. Kim, I. Park, K. D. Yang, H.-Y. Jeong, J. Kim, K. T. Hong, H. W. Jang, K. Kang and K. T. Nam, *Journal of the American Chemical Society*, 2014, **136**, 4201-4211.
- G. He, G. Popov and L. F. Nazar, *Chemistry of Materials*, 2013, **25**, 1024-1031.
- G. Zhong, Y. Li, P. Yan, Z. Liu, M. Xie and H. Lin, *The Journal of Physical Chemistry C*, 2010, **114**, 3693-3700.
- C. Lyness, B. Delobel, A. R. Armstrong and P. G. Bruce, *Chemical Communications*, 2007, 4890-4892.
- A. R. Armstrong, C. Lyness, M. Ménétrier and P. G. Bruce, *Chemistry of Materials*, 2010, **22**, 1892-1900.
- H. H. Sumathipala, M. A. K. L. Dissanayake and A. R. West, *Solid State Ionics*, 1996, **86-88, Part 2**, 719-724.
- A. R. West and F. P. Glasser, *Journal of Solid State Chemistry*, 1972, **4**, 20-28.
- B. Monnaye, C. Garraut, G. Perez and R. Bouaziz, *CR Seances Acad Sci Ser C*, 1974, **278**, 251.
- P. Tarte and R. Cahay, *CR Seances Acad Sci Ser C*, 1970, **271**, 777.
- B. Toby, *Journal of Applied Crystallography*, 2001, **34**, 210-213.
- S. Jin, A. G. Hubert, Y. Naoaki and S.-H. Yang, *J. Electrochem. Soc.*, 2010, **157**, B1263-B1268.
- H. Jia, J. Stark, L. Q. Zhou, C. Ling, T. Sekito and Z. Markin, *RSC Advances*, 2012, **2**, 10874-10881.
- G. Kresse and D. Joubert, *Phys. Rev. B*, 1999, **59**, 1758-1775.
- G. Kresse and J. Furthmüller, *Phys. Rev. B*, 1996, **54**, 11169-11186.
- G. Kresse and J. Furthmüller, *Computational Materials Science*, 1996, **6**, 15-50.
- G. Kresse and J. Hafner, *Phys. Rev. B*, 1994, **49**, 14251-14269.
- T. Mueller, G. Hautier, A. Jain and G. Ceder, *Chemistry of Materials*, 2011, **23**, 3854-3862.
- R. Shannon, *Acta Crystallographica Section A*, 1976, **32**, 751-767.
- E. Plattner, H. Völlenke and A. Wittmann, *Monatshefte für Chemie*, 1976, **107**, 921-927.
- A. J. Esswein, M. J. McMurdo, P. N. Ross, A. T. Bell and T. D. Tilley, *Journal of Physical Chemistry C*, 2009, **113**, 15068-15072.
- F. Jiao and H. Frei, *Angew. Chem. Int. Ed.*, 2009, **48**, 1841-1844.
- J. B. Gerken, J. G. McAlpin, J. Y. C. Chen, M. L. Rigsby, W. H. Casey, R. D. Britt and S. S. Stahl, *J. Am. Chem. Soc.*, 2011, **133**, 14431-14442.
- J. G. McAlpin, Y. Surendranath, M. Dinca, T. A. Stich, S. A. Stoian, W. H. Casey, D. G. Nocera and R. D. Britt, *J. Am. Chem. Soc.*, 2010, **132**, 6882-6883.
- B. J. Tan, K. J. Klabunde and P. M. A. Sherwood, *Journal of the American Chemical Society*, 1991, **113**, 855-861.
- A. Foelske and H. H. Strehblow, *Surf. Interface Anal.* 2002, **34**, 125-129.
- A. Foelske and H. H. Strehblow, *Surf. Interface Anal.* 2000, **29**, 548-555.
- A. Foelske, J. Kunze and H. H. Strehblow, *Surf. Sci.* 2004, **554**, 10-24.

Journal Name

38. K. J. McDonald and K-S. Choi, *Chemistry of Materials*, 2011, **23**, 1686-1693.
39. J. A. Koza, C. M. Hull, Y.-C. Liu and J. A. Switzer, *Chemistry of Materials*, 2013, **25**, 1922-1926.
40. M. J. N. Pourbaix, *Atlas of Electrochemical Equilibria in Aqueous Solutions*. 2nd ed, Natl. Assoc. Corrosion Eng., Houston, Texas, 1974.

Table of content entry

We report hydrothermal synthesis and structural refinement of $\text{Li}_2\text{CoGeO}_4$, as well as its use as catalyst for oxygen evolution reaction.

